Computational Materials Science 142 (2018) 290–296

Contents lists available at ScienceDirect

Computational Materials Science

journal homepage: www.elsevier.com/locate/commatsci

Radiation tolerance of nanotwinned metals – An atomistic perspective

Shuyin Jiao, Yashashree Kulkarni *

Department of Mechanical Engineering, University of Houston, Houston, TX 77204, USA

ARTICLE INFO

Article history:
Received 12 July 2017
Received in revised form 9 October 2017
Accepted 12 October 2017

Keywords:
Twin boundaries
Radiation
Nanotwinned metals
Molecular dynamics

ABSTRACT

Remarkable properties of ultra-high strength, ductility, and stability have been achieved through the introduction of twin boundaries in nanostructured metals. Here, we report molecular dynamics simulations which elucidate the synergistic role of grain boundaries and twin boundaries in enhancing the radiation tolerance of nanotwinned metals. While grain boundaries are known to be excellent sinks for point defects, coherent twin boundaries do not absorb point defects. A beneficial corollary is that the structural integrity of coherent twin boundaries remains intact as radiation-induced defects pass through them and ultimately get absorbed into grain boundaries. Hence, the twin boundaries can continue to play a role in imparting high strength even after being subjected to irradiation. Thus, nanotwinned structures may indeed be optimal motifs for radiation tolerant materials that preserve high strength and ductility.

1. Introduction

The optimal design of structural materials that can sustain radiation damage while achieving high strength and toughness is an important challenge for future nuclear power systems. Continued exposure to extreme environments due to neutron, proton, and heavy ion irradiation can eventually lead to material degradation thereby raising safety and reliability concerns [1]. The atomistic origin of material damage due to irradiation lies in the formation of vacancies and interstitials. The migration and interaction of these point defects lead to further damage which includes formation of voids, stacking fault tetrahedra (SFTs), and dislocation loops as these vacancies and interstitials coalesce into clusters. Material swelling occurs as interstitials migrate to the surface, while interstitial aggregates act as obstacles to dislocation motion resulting in embrittlement of the material [2,3].

It is well established that grain boundaries (GBs) improve radiation resistance by serving as excellent sinks for radiation-induced point defects [4,5]. Compared to their coarser counterparts, nanocrystalline materials have a much higher volume fraction of GBs which imparts greater strength as well as resistance to radiation. This has led to extensive experimental and computational studies on nanocrystalline materials as radiation-tolerant materials [6–11]. However, the increase in strength and radiation-tolerance of nanocrystalline materials with decreasing grain size comes with severe issues such as loss of ductility, creep, and grain growth which weaken their case for critical structural applications [12]. In contrast, research has provided compelling evidence for the ultra-high strength of nanotwinned metals while preserving ductility, and grain stability [13–19]. These remarkable properties are attributed to twin boundaries that strengthen by arresting dislocation motion and retain ductility by accommodating plastic strain. Naturally then, there is a growing interest in investigating the radiation response of nanotwinned metals. Recent experimental and computational studies have elucidated the interaction of radiation-induced defects with twin boundaries. Demkowicz et al. [20] showed that coherent twin boundaries (CTBs) are poor sinks for point defects through molecular dynamics simulations. They speculated that CTBs could speed up defect recombination and thereby lead to significantly lower number of radiation-induced defects compared to single crystals. Recently, Yu et al. [21] found from experiments that coherent and incoherent TBs in face-centered-cubic (fcc) metals could annihilate radiation-induced SFTs at room temperature. They also reported migration of incoherent TBs under irradiation.

In this paper, we report molecular dynamics simulations which elucidate the complementary role of grain boundaries and twin boundaries in enhancing the radiation tolerance of nanotwinned metals. To this end, we first perform cascade simulations on columnar specimens comprising of both twin boundaries and general grain boundaries. We then perform uniaxial tension simulations to investigate the deformation response of nanotwinned and nanocrystalline specimens subjected to radiation damage. We find that radiation-induced defects can pass through CTBs without distorting the structure of the CTBs and are ultimately absorbed by GBs leaving the intragranular regions with fewer defects. Thus, the results discussed here together with previous

* Corresponding author.
E-mail address: ykulkarni@uh.edu (Y. Kulkarni).

https://doi.org/10.1016/j.commatsci.2017.10.023
0927-0256/

studies suggest that an optimal volume fraction of GBs and TBs, based on the grain size and twin lamella thickness, could make nanotwinned metals potential candidates as radiation-resistant materials with excellent mechanical properties.

2. Simulation method

Molecular dynamics simulations were performed on columnar specimen of fcc copper consisting of four hexagonal grains. As shown in Fig. 1, the orientation of grain 1 was along the $[1\,1\,\bar{2}]$, $[1\,1\,1]$ and $[1\,\bar{1}\,0]$ crystallographic directions. Grains 2, 3 and 4 were rotated around the $[1\,\bar{1}\,0]$ axis by 30°, 60° and 90° respectively in the X-Y plane. The digital specimens had a size of $35 \times 40 \times 20$ nm, and consisted of about 2,370,000 atoms. The diameter of each grain was about 20 nm. Nanotwinned specimens were constructed by inserting CTBs in each grain. Five different twin spacings were considered, specifically, 0.6 nm, 1.2 nm, 2.5 nm, 5 nm, and 10 nm. The results for these cases were compared with those for the nanocrystalline specimen without CTBs and single crystal specimen. Periodic boundary conditions were specified in all directions. The initial equilibrium structure of each specimen was obtained using conjugate gradient energy minimization. Fig. 1 shows the relaxed atomistic structure of a specimen containing CTBs with a spacing of 5 nm after energy minimization. The atomic interactions were modeled using the embedded atom (EAM) interatomic potential developed by Mishin et al. [22]. The ZBL repulsive potential [23] was splined to the EAM potential for atomic distances smaller than 0.5 Å to prevent atoms from coming unrealistically close during radiation cascades.

After energy minimization, each specimen was equilibrated at 300 K under the NPT ensemble for 100 ps. The radiation simulation was started by selecting four primary knock-on atoms (PKA) and giving certain amount of kinetic energy to each of them in order to initiate radiation cascades in the system. Simulations were performed for two different PKA energies, namely, 10 keV and 20 keV. Since the results for both cases are qualitatively similar, we discuss the 10 keV simulations in the main text of the paper and defer the 20 keV results to the Supplementary Material [24]. As shown in Fig. 1, PKA 1 and 3 were located about 48 Å away from the nearest GBs, and PKA 2 and 4 were located about 25 Å away from the nearest GBs. The specific positions of the PKA were chosen such that PKA 1 and 3 impinged on the CTBs first, whereas PKA 2 and 4 impinged directly on the GBs. The velocity for each PKA was chosen to be perpendicular and directed toward its nearest interface. The cascades were equilibrated in the NVE ensemble for 2 ps using a timestep of 0.1 fs and for another 1000 ps using a timestep of 2 fs. Steady state was observed to have reached after about 562 ps when the defect structure appeared stable with no significant changes on the time-scale of molecular dynamics. During the simulation, the outermost layers of atoms of the three-dimensional simulation box were fixed to rescale their velocities for dissipating the energy and maintaining the temperature of the system at 300 K. After irradiation, the irradiated and pristine specimens were subjected to tensile loading. To this end, each system was relaxed for 100 ps at 300 K under the NPT ensemble. Then, the structure was subjected to a tensile deformation along the X direction with a strain rate of $4 \times 10^8\ s^{-1}$ for 300 ps under the NVT ensemble. All simulations were performed using the molecular dynamics code, LAMMPS [25]. Defects were visualized using common neighbor analysis [26] in OVITO [27] and AtomEye [28].

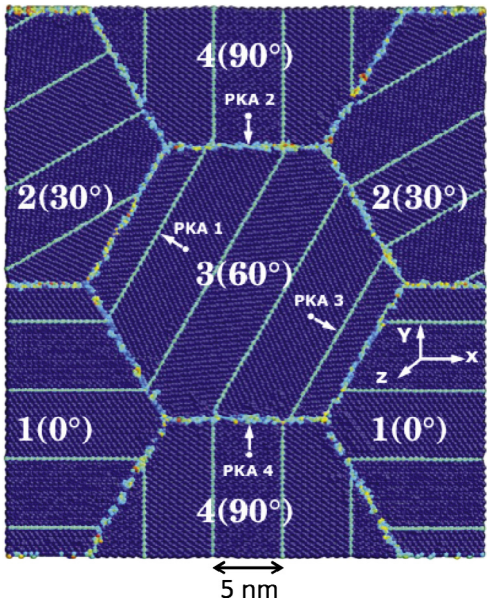

Fig. 1. Equilibrium configuration of columnar nanotwinned Cu with grain size of 20 nm and CTB spacing of 5 nm.

3. Results and discussion

3.1. Radiation response of nanotwinned copper

Fig. 2 shows radiation cascades generated in two representative specimens, specifically, nanocrystalline Cu and nanotwinned Cu with a CTB spacing of 1.2 nm. The kinetic energy imparted to each PKA is 10 keV. The fcc atoms in perfect crystal structure are not shown in order to identify the defects. A large number of atoms are displaced from their initial lattice positions leading to four displacement cascade events due to the four PKAs. Comparing Fig 2a and b, it is interesting to note that most of the twin boundary structure (shown by the rows of red atoms) is still maintained even during the cascade event.

Fig. 3 shows equilibrated structures of the single crystalline, nanocrystalline and nanotwinned specimens using common neighbor analysis. The snapshots are taken at 562 ps after cascade initiation. Blue atoms are in body-centered cubic (bcc) configuration, red atoms are in hexagonal-closed-packed (hcp) configuration and cyan atoms cannot be in classified as fcc, bcc, or hcp. Fcc atoms are not shown. Compared to Fig. 2, most of the displaced atoms recover their perfect lattice positions during equilibration leaving behind various defects that include single vacancies (identified as 12-neighbor clusters), small vacancy clusters, stacking faults, and SFTs. ⟨0 0 1⟩ dumbbells characterized by two interstitials and one vacancy are also observed in all specimens. The dumbbells are stable defects and are seen to move freely within the intragranular regions. Some of these defects are marked in Fig. 3(b) for further clarity. Looking at Fig. 3(a)–(f), we note that the precise defect structures after relaxation are governed by the shape and spread of the radiation cascade which in turn are quite sensitive to a number of factors including PKA direction and energy, the specimen microstructure, as well as the initial velocity distribution of the atoms corresponding to the prescribed temperature. Thus, comparing the specific distribution of radiation-induced defects in different cases is not quite useful. Nevertheless, the simulations furnish two interesting (and related) insights about CTBs. Consistent with prior studies [20], we find that CTBs are indeed poor sinks for radiation-induced defects. In fact, these defects are able to pass through the CTBs without causing any significant distortion. Many of these defects, especially interstitials, ultimately get absorbed by the GBs which are known to be excellent sinks for point defects. A rather unexpected consequence of this property

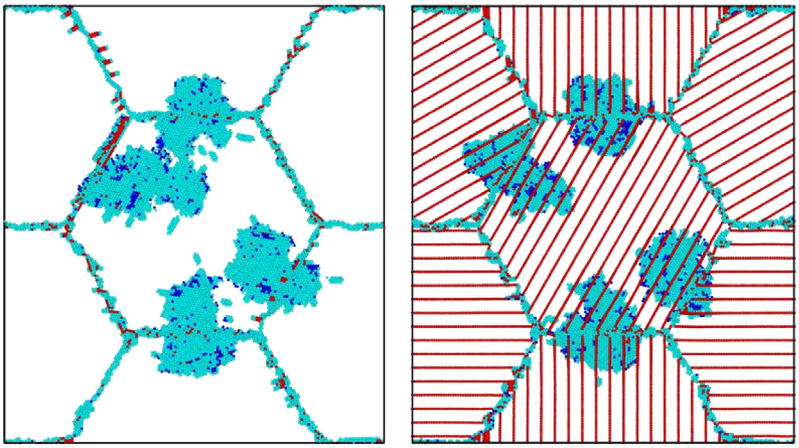

Fig. 2. Defective structures at 0.5 ps after cascade initiation due to irradiation of (a) Nanocrystalline Cu; and (b) Nanotwinned Cu with CTB spacing of 1.2 nm. Blue: BCC, Red: HCP, Cyan: Others. (For interpretation of the references to colour in this figure legend, the reader is referred to the web version of this article.)

of CTBs is that the structural integrity of the CTBs remains intact even after these point defects and dumbbells pass through them. Fig. 4 shows a dumbbell moving through a CTB during equilibration leaving the structure of the CTB defect-free as before. This is in sharp contrast to GBs whose interfacial structure is heavily distorted as they absorb more and more defects and eventually become favorable sites for dislocation nucleation. This can be observed by comparing the structure of the GBs enclosing the central grain in Fig. 3 to their initial structure in Fig. 1.

Fig. 5 shows the distribution of interstitials and vacancies in nanocrystalline and nanotwinned specimens extracted using the Wigner-Seitz defect analysis implemented in OVITO [27]. Red color denotes interstitials and blue denotes vacancies. A vacancy is identified as an empty Wigner-Seitz cell whereas an interstitial is identified as a cell with multiple atoms [29]. Based on the color coding, we observe that the point defects concentrated in the GB regions are mostly interstitials and those left within the grain are mostly vacancies. This is consistent with existing studies which show that interstitials are absorbed by GBs and the primary defects left within the grains are vacancies that eventually form clusters, stacking faults and SFTs [11,9,21]. Similar defect distribution in nanotwinned specimens (Fig. 5(b)) confirms that the interstitials can indeed traverse multiple CTBs in the intragranular region to be absorbed by the enclosing GBs.

Fig. 6 shows the distribution of radiation-induced defects left within the central grain (excluding a few atomic layers around the GB region) in different specimens using the reference lattice site method. This method estimates the number of point defects in a region by calculating the difference between an atom's current coordinates and coordinates in the initial reference configuration before irradiation [11]. We find that the nanocrystalline specimen has 202 interstitials and 296 vacancies, the nanotwinned specimen with 1.2 nm CTB spacing has 63 interstitials and 105 vacancies while the nanotwinned specimen with 0.6 nm CTB spacing has 21 interstitials and 69 vacancies. The decrease in the number of residual point defects with decreasing CTB spacing is consistent with both experimental and computational studies in the literature. Based on their atomistic simulations, Demkowicz et al. [20] showed that the radiation-induced Frenkel pairs have a greater tendency for recombination in the vicinity of CTBs. Based on their in situ radiation studies inside a TEM microscope, Jin et al. [30] hypothesized that point defects may diffuse rapidly along TBs and then recombine with point defects of the opposite type.

In addition, the number of interstitials in the grain is less than the number of vacancies in all cases, which further supports the observation that more interstitials are absorbed into GBs. However, it should be noted that the number of interstitials and vacancies calculated for all the cases is somewhat larger than actual because the reference lattice site method does not distinguish between free or single point defects and those interstitials and vacancies that are part of clusters such as SFTs. Nevertheless, the estimates are useful for a relative comparison which certainly indicates that the total number of point defects and defect clusters in the nanotwinned specimens are less than that in the nanocrystalline specimen. In addition, when the twin spacing is 0.6 nm, we note that the size of the SFT is smaller than those formed in other specimens with larger or no twins. This is consistent with the radiation simulations involving 20 keV PKAs [24]. In the latter case, the specimens with the smaller CTB spacings display less defect clustering and show vacancies and dumbbells distributed throughout the intragranular region (Fig. S4 in [24]) as compared to the single crystalline and nanocrystalline specimens. Thus, we speculate that CTBs can possibly prevent point defects from clustering and a higher density of twins may lead to smaller defect clusters. However, we note that this is a conjecture based on our present simulations and a quantitative analysis would require further investigation. Nevertheless, our preliminary MD predictions are corroborated by experimental data recently reported by Zhang and coworkers [31,32]. They observe that finer twin spacing leads to lower density of defect clusters in both nanotwinned Ag and nanotwinned Cu.

3.2. Tensile deformation of irradiated nanotwinned copper

In order to understand the mechanical response of nanotwinned metals subjected to radiation damage, we perform simulations of tensile tests on irradiated specimens as described previously in Section 2. Fig. 7 shows the stress versus strain curves for the various irradiated samples in uniaxial tension. For the sake of comparison, we also show tensile stress versus strain curves for unirradiated nanocrystalline and nanotwinned Cu. We note that even after irradiation, the peak stresses for all specimens are in the same range around 2 GPa which is significantly high. Compared with unirradiated counterparts, we find that the strength of irradiated specimens is equal or only marginally lower than the strength before radiation damage. Interestingly, this is also true when the specimens are subjected to 20 keV PKAs, and naturally, have a larger number and spread of radiation-induced defects (Fig. S5 in [24]). A possible reason for the slight decrease in the strength of irradiated specimen is that the GBs distorted with the absorption of interstitials offer favorable sites for dislocation

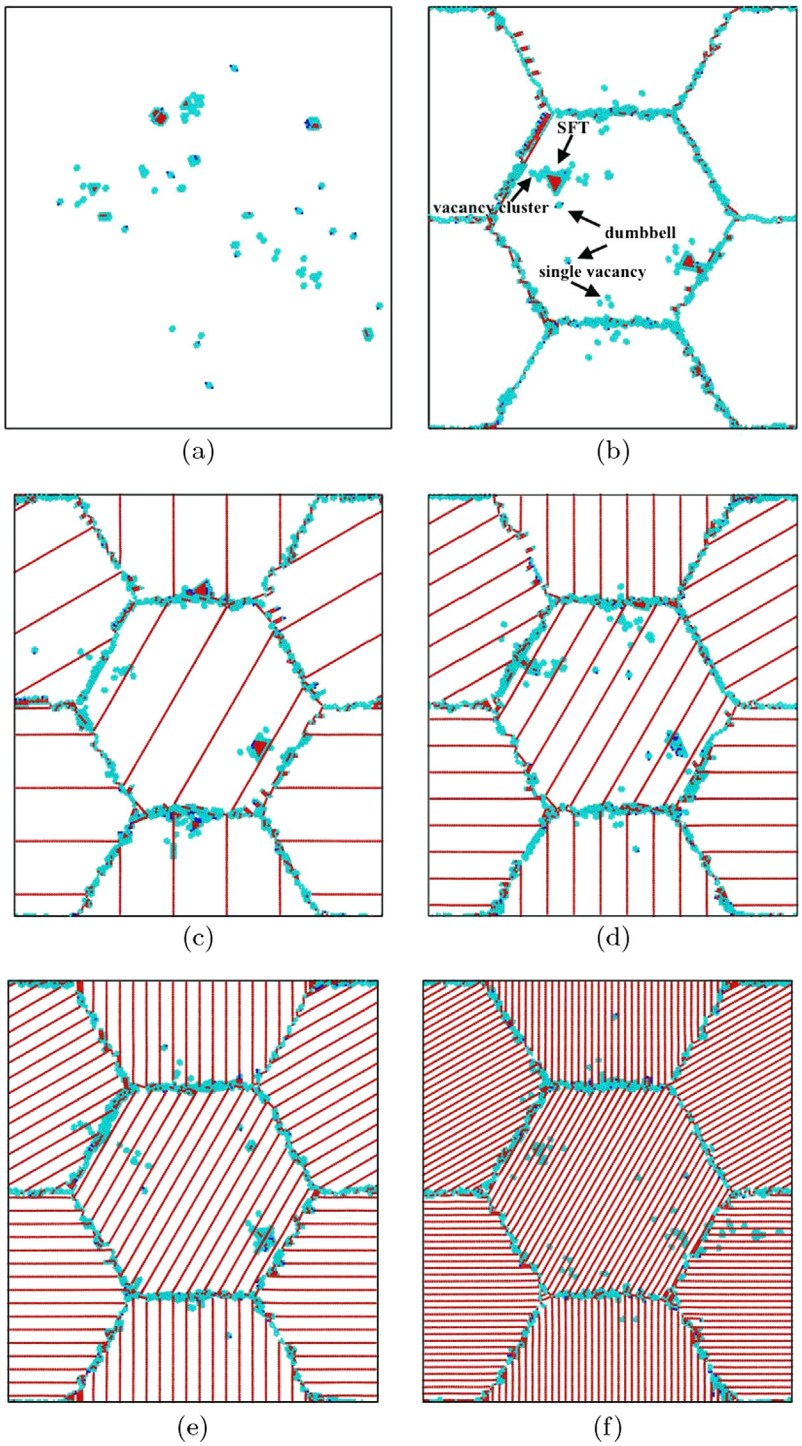

Fig. 3. Defect structures at 562 ps after cascade initiation due to four 10 KeV PKAs of (a) Single crystal Cu; (b) Nanocrystalline Cu; (c) Nanotwinned Cu with CTB spacing of 5 nm; (d) Nanotwinned Cu with CTB spacing of 2.5 nm; (e) Nanotwinned Cu with CTB spacing of 1.2 nm; (f) Nanotwinned Cu with CTB spacing of 0.6 nm. Blue: BCC, Red: HCP, Cyan: Others. (For interpretation of the references to colour in this figure legend, the reader is referred to the web version of this article.)

nucleation. We also note that in Fig. 7, the yield stress (the stress at which the first dislocation is nucleated) for nanocrystalline Cu is found to be greater than the nanotwinned Cu samples which have CTB spacing of 2.5 nm or less. We believe that this may be due to the greater density of CTBS in these specimens and hence more number of CTB-GB intersections which offer more sites for dislocation nucleation along CTBs. This is in fact consistent with the softening observed by Li et al. [33] for smaller CTB spacing and attributed to nucleation of partials parallel to CTBs. On the other hand, Fig. S5 [24] compares the yield and peak stresses of nanocrystalline Cu and nanotwinned Cu with CTB spacing larger than 2.5 nm. In this case, only the nanotwinned Cu with CTB spacing of 2.5 nm shows lower yield stress. The yield stress of nanotwinned Cu with CTB spacing of 5 nm and 10 nm is not very different from nanocrystallline Cu.

As a representative example, Fig. 8 shows the microstructural evolution of nanotwinned Cu with 1.2 nm CTB spacing subjected to tension after irradiation. It is rather interesting to note that both

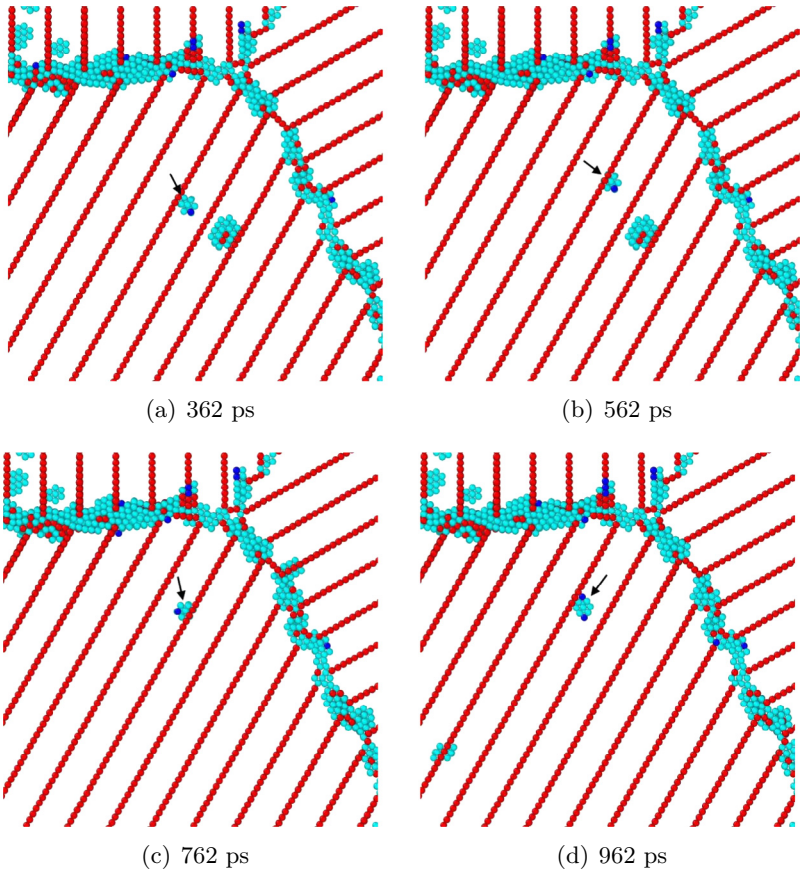

Fig. 4. Atomistic images showing a dumbbell crossing a CTB during equilibration after radiation cascade. Blue: BCC, Red: HCP, Cyan: Others). (For interpretation of the references to colour in this figure legend, the reader is referred to the web version of this article.)

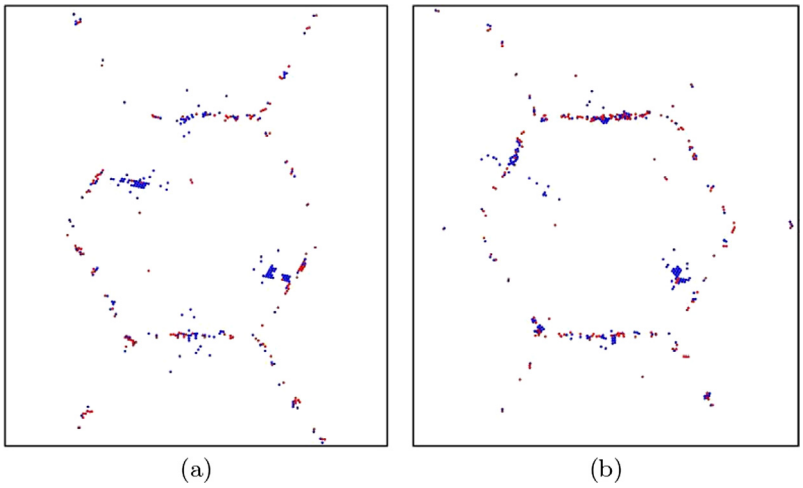

Fig. 5. Wigner-Seitz defect analysis of specimen after irradiation (Red: Interstitial, Blue: Vacancy). (a) Defect configuration of nanocrystalline Cu at 562 ps after cascade initiation; (b) Defect configuration of nanotwinned Cu with CTB spacing of 1.2 nm at 562 ps after cascade initiation. (For interpretation of the references to colour in this figure legend, the reader is referred to the web version of this article.)

unirradiated and irradiated specimens exhibit nucleation and propagation of the leading partial dislocations from triple junctions and GB regions with trailing stacking faults [34]. In comparison, as shown in Fig. S6(a) and (b) in [24], different slip systems may be activated in nanocrystalline Cu (with no CTBs) with or without radiation-induced defects under similar tensile loading conditions. Moreover, other slip systems also get activated in nanotwinned Cu with larger twin spacing (2.5 nm or larger) (see Fig. S6(d) in [24]). However, Figs. 8, S2, and S6(c) reveal that in the case of nanotwinned Cu with 2.5 nm CTB spacing or less, most stacking faults are found to nucleate parallel to the existing CTBs. Taken together, this probably indicates that the presence of the GB-CTB junctions, which offer sites for dislocation nucleation, play a more dominant role than the Schmid factor for the different slip systems [35] in governing the deformation mechanism. When the CTB spacing is large, there are not enough GB-CTB junctions for defect nucleation,

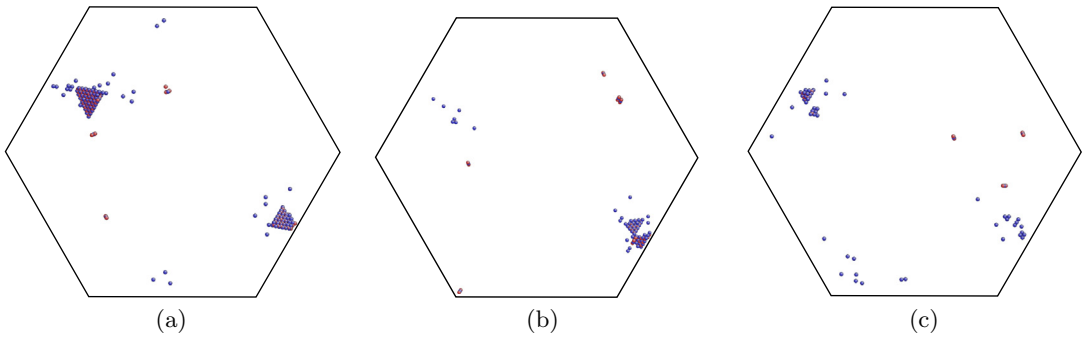

Fig. 6. Defect distribution after radiation in the central grain of (a) nanocrystalline Cu; (b) nanotwinned Cu with CTB spacing of 1.2 nm; (c) nanotwinned Cu with CTB spacing of 0.6 nm. Red indicates displaced atoms and blue indicates a vacant site. (For interpretation of the references to colour in this figure legend, the reader is referred to the web version of this article.)

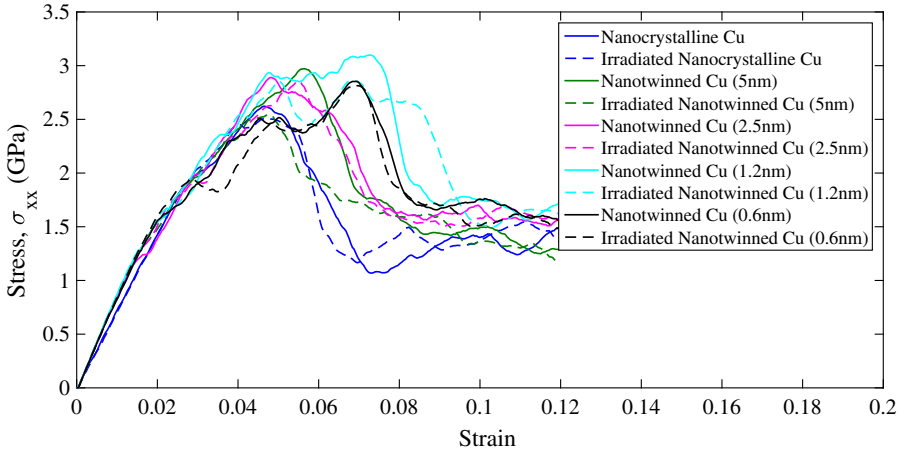

Fig. 7. Comparison on tension response of nanocrystalline Cu and nanotwinned Cu before and after radiation.

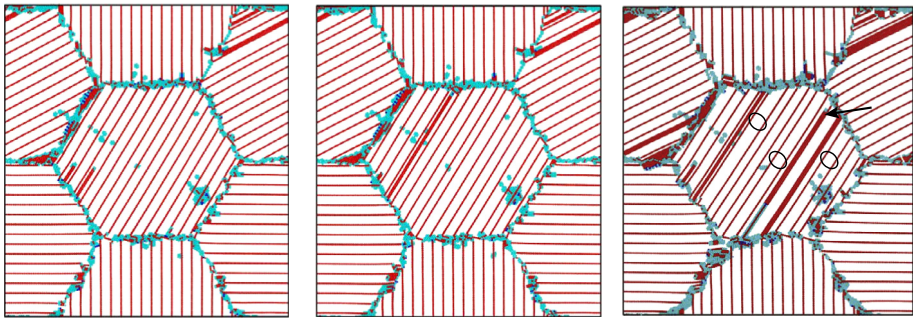

Fig. 8. Defect evolution in nanotwinned Cu with 1.2 nm CTB spacing during tension after irradiation. (a) SFs nucleating from a GB; (b) SFs extend through the grain; (c) Twin boundary migration; The arrow points to a Shockley partial dislocation moving along a CTB which leads to migration of the CTB by one atomic layer. The circles indicate an increase in TB spacing in some places due to TB migration.

and hence other slip systems can get activated based on the critical resolved shear stress. Our analysis is also consistent with the observation reported by Li et al. [33], based on their simulations of 3D and columnar nanotwinned Cu, that there is a transition to nucleation of partials along CTBs when the twin spacing goes below 2.5 nm in an average grain size of 20 nm. At larger strains, twin boundary migration is found to occur in both irradiated and unirradiated specimens as stacking faults nucleate on planes adjacent to CTBs. The CTB migration is indicated in Fig. 8(c) and occurs by the motion of Shockley partials along CTBs. Point defects, dumbbells, and small vacancy clusters in the intragranular region do not play a major role in governing plasticity. Eventually, the radiation-induced SFTs within the grains also become sources of dislocations. We wish to note that radiation-induced twin boundary migration is not observed in our simulations unlike that reported in many experimental studies on nanotwinned Cu and Ag [21,36,37]. Perhaps this is due to the fact that our digital specimens contain defect-free coherent twin boundaries whereas the experimental studies primarily observe migration of incoherent twin boundaries during irradiation. Furthermore, our simulation time for observing radiation damage is limited to about few hundred picoseconds due to the time scale of molecular dynamics. Hence, phenomena involving slow atomistic processes, such as diffusion of defects, are inaccessible through molecular dynamics.

4. Conclusions

In summary, we report our study of the radiation response of nanotwinned fcc metals by way of molecular dynamics simulations. The simulations reveal a synergy between the distinct roles of grain boundaries and twin boundaries in enhancing the radiation tolerance of nanotwinned structures. As is well-established, grain boundaries serve as excellent sinks for radiation-induced point defects. In contrast, coherent twin boundaries are poor sinks for point defects. As a result, our simulations reveal that point defects and dumbbells can pass through multiple twin boundaries and are ultimately absorbed by grain boundaries. An intriguing consequence of this is that the structure of coherent twin boundaries remains intact during irradiation. Taken together, the study indicates that grain boundaries enhance radiation tolerance by absorbing radiation-induced defects while the coherent twin boundaries, with their undistorted structure, continue to play their role in enhancing strength and ductility of nanotwinned metals. We wish to note that our MD simulations are limited by their grain sizes and time scales and hence they are unable to capture all the deformation mechanisms reported in experimental studies. Nevertheless, the key mechanisms associated with twin boundaries observed in our simulations are consistent with several experimental findings. The atomistic underpinning of the observation that twin boundaries may lead to reduced point defect density and smaller defect clusters is worth investigating further. This can have important ramifications for the application of nanotwinned structures as radiation tolerant materials. To this end, investigating the migration and interaction of radiation-induced point defects with coherent and incoherent twin boundaries over realistic time scales using novel time-scaling computational approaches offers an exciting avenue for future work.

Acknowledgment

The authors would like to acknowledge the support of the US National Science Foundation under grant CMMI-1129041. The authors also acknowledge the use of the Maxwell cluster and the support from the Center of Advanced Computing and Data Systems at the University of Houston to carry out the research presented here.

Appendix A. Supplementary material

Supplementary data associated with this article can be found, in the online version, at https://doi.org/10.1016/j.commatsci.2017.10.023.

References

[1] S.J. Zinkle, G.S. Was, Acta Mater. 61 (2013) 735.
[2] G. Ackland, Science 327 (2010) 1587.
[3] M.J. Demkowicz, P. Bellon, B.D. Wirth, MRS Bull. 35 (2010) 992.
[4] B.N. Singh, Philos. Magaz. 29 (1974) 25.
[5] K. Sugio, Y. Shimomura, T.D. de la Rubia, J. Phys. Soc. Japan 67 (1998) 882.
[6] M. Rose, A.G. Balogh, H. Hahn, Nucl. Instrum. Methods Phys. Res. B 127 (1997) 119.
[7] N. Nita, R. Schaeublin, M. Victoria, R.Z. Valiev, Philos. Magaz. 85 (2005) 723.
[8] Y. Chimi, A. Iwase, N. Ishikawa, M. Kobiyama, T. Inami, S. Okuda, J. Nucl. Mater. 297 (2001) 355.
[9] M. Samaras, P.M. Derlet, H. Van Swygenhoven, M. Victoria, Phys. Rev. Lett. 88 (2002) 125505.
[10] S. Wurster, R. Pippan, Scripta Mater. 60 (2009) 1083.
[11] X.M. Bai, A.F. Voter, R.G. Hoagland, M. Nastasi, B.P. Uberuaga, Science 327 (2010) 1631.
[12] M. Dao, L. Lu, R.J. Asaro, J.T.M. De Hossan, E. Ma, Acta Mater. 55 (2007) 4041.
[13] L. Lu, Y.F. Shen, X.H. Chen, L.H. Qian, K. Lu, Science 304 (2004) 422.
[14] T. Zhu, J. Li, A. Samanta, H.G. Kim, S. Suresh, PNAS 104 (2007) 3031.
[15] L. Lu, X. Chen, X. Huang, K. Lu, Science 323 (2009) 607.
[16] Y. Kulkarni, R.J. Asaro, D. Farkas, Scripta Mater. 60 (2009) 532.
[17] J. Bezares, S. Jiao, Y. Liu, D. Bufford, L. Lu, X. Zhang, Y. Kulkarni, R.J. Asaro, Acta Mater. 60 (2012) 4623.
[18] Y.M. Wang, F. Sansoz, T. LaGrange, R.T. Ott, J. Marian, T.W. Barbee Jr., A.V. Hamza, Nat. Mater. 12 (2013) 697.
[19] H. Mirkhani, S.P. Joshi, J. Mech. Phys. Solids 68 (2014) 107.
[20] M. Demkowicz, O. Anderoglu, X. Zhang, A. Misra, J. Maters. Res. 26 (2011) 1666.
[21] K.Y. Yu, D. Bufford, C. Sun, Y. Liu, H. Wang, M.A. Kirk, M. Li, X. Zhang, Nat. Commun. 4 (2013) 1377.
[22] Y. Mishin, M.J. Mehl, D.A. Papaconstantopoulos, A.F. Voter, J.D. Kress, Phys. Rev. B. 63 (2001) 224106.
[23] J.F. Ziegler, J.P. Biersack, U. Littmark, The stopping and range of ions in matter, 1 (1985).
[24] See supplementary material for details of radiation and tensile simulations for the various specimens studied in this work.
[25] S.J. Plimpton, J. Comp. Phys. 117 (1995) 1.
[26] J.D. Honeycutt, H.C. Andersen, J. Phys. Chem. 91 (1987) 4950.
[27] A. Stukowski, Model. Simul. Mater. Sci. Eng. 18 (2010) 015012.
[28] J. Li, Model. Simul. Mater. Sci. Eng. 11 (2003) 173.
[29] F. Gao, W.J. Weber, Phys. Rev. B 66 (2002) 024106.
[30] J. Li, K.Y. Yu, Y. Chen, M. Song, H. Wang, M.A. Kirk, M. Li, X. Zhang, Nano Lett. 15 (2015) 2922.
[31] Y. Chen, J. Li, K.Y. Yu, H. Wang, M.A. Kirk, M. Li, X. Zhang, Acta Mater. 111 (2016) 148.
[32] J. Li, Y. Chen, H. Wang, X. Zhang, Metall. Mater. Trans. A 48 (2017) 1466.
[33] X. Li, Y. Wei, L. Lu, K. Lu, H. Gao, Nature 464 (2010) 877.
[34] Z.X. Wu, Y.W. Zhang, D.J. Srolovitz, Acta Mater. 57 (2009) 4508.
[35] V. Borovikov, M.I. Mendelev, A.H. King, R. LeSar, J. Appl. Phys. 117 (2015) 085302.
[36] K.Y. Yu, D. Bufford, F. Khatkhatay, H. Wang, M.A. Kirk, X. Zhang, Scripta Mater. 69 (2013) 385.
[37] Y. Chen, H. Wang, M.A. Kirk, M. Li, J. Wang, X. Zhang, Scripta Mater. 130 (2017) 37.